Title

Molecular Architecture of Photoreceptor Phosphodiesterase Elucidated by Chemical Cross-Linking and Integrative Modeling

Journal

Journal of Molecular Biology, 426(22)

ISSN

0022-2836

Authors

Zeng-Elmore, Xiaohui
Gao, Xiong-Zhuo
Pellarin, Riccardo
et al.

Publication Date

2014-11-01

DOI

10.1016/j.jmb.2014.07.033

Peer reviewed

Published in final edited form as:
J Mol Biol. 2014 November 11; 426(22): 3713–3728. doi:10.1016/j.jmb.2014.07.033.

Molecular architecture of photoreceptor phosphodiesterase elucidated by chemical cross-linking and integrative modeling

Xiaohui Zeng-Elmore[1,2,†], **Xiong-Zhuo Gao**[1,†], **Riccardo Pellarin**[3], **Dina Schneidman-Duhovny**[3], **Xiu-Jun Zhang**[1], **Katie A. Kozacka**[1], **Yang Tang**[1,2], **Andrej Sali**[3,4,5], **Robert J. Chalkley**[4], **Rick H. Cote**[1], and **Feixia Chu**[1,2,*]

[1]Department of Molecular, Cellular & Biomedical Sciences, University of New Hampshire, Durham, NH 03824

[2]Hubbard Center for Genome Studies, University of New Hampshire, Durham, NH 03824

[3]Department of Bioengineering and Therapeutic Sciences, University of California, San Francisco

[4]Department of Pharmaceutical Chemistry, University of California, San Francisco

[5]California Institute for Quantitative Biosciences, University of California, San Francisco, CA 94158

Abstract

Photoreceptor phosphodiesterase (PDE6) is the central effector enzyme in visual excitation pathway in rod and cone photoreceptors. Its tight regulation is essential for the speed, sensitivity, recovery and adaptation of visual detection. Although major steps in the PDE6 activation/deactivation pathway have been identified, mechanistic understanding of PDE6 regulation is limited by the lack of knowledge about the molecular organization of the PDE6 holoenzyme ($\alpha\beta\gamma\gamma$). Here, we characterize the PDE6 holoenzyme by integrative structural determination of the PDE6 catalytic dimer ($\alpha\beta$), based primarily on chemical cross-linking and mass spectrometric analysis. Our models built from the high-density cross-linking data elucidate a parallel organization of the two catalytic subunits, with juxtaposed α-helical segments within the tandem regulatory GAF domains to provide multiple sites for dimerization. The two catalytic domains exist in an open configuration when compared to the structure of PDE2 in the *apo* state. Detailed structural elements for a differential binding of the γ-subunit to the GAFa domains of the α- and β-subunit are revealed, providing insight into the regulation of the PDE6 activation/deactivation cycle.

*To whom correspondence should be addressed. feixia.chu@unh.edu.
†Contributed equally to this study.

Keywords

phosphodiesterase 6 (PDE6); chemical cross-linking; mass spectrometry; integrative modeling; visual transduction

Introduction

The vertebrate visual excitation and recovery are mediated by intricately connected protein complexes localized to the disk membranes in the outer segments of photoreceptor cells (1, 2). Vision begins with the photoactivation of visual pigment, opsin, which sets in motion a highly amplified visual excitation pathway. This G-protein coupled receptor activates multiple copies of transducin, each of which interacts with a photoreceptor-specific cyclic nucleotide phosphodiesterase (PDE6) and relieves its inhibition. Hydrolysis of cGMP catalyzed by PDE6 causes the closure of cGMP-gated ion channels, leading to outer segment membrane hyperpolarization and vision initiation. The lifetime of PDE6 activation is determined by the GTPase activity of transducin α-subunit ($G\alpha_t$), which is further accelerated by a G-protein signaling 9 (RGS9) protein complex (3). The physiological importance of precisely regulating PDE6 activity is demonstrated by the fact that deleterious PDE6 mutations are common causes of autosomal recessive retinitis pigmentosa, a progressive retinal degenerative disease (4).

The rod and cone photoreceptor isoforms of PDE6 are but one of eleven families of vertebrate PDEs that share a highly conserved catalytic domain (5). Five of the PDE6 families (including PDE6) have an N-terminal regulatory region, consisting of a tandem GAF domain (GAFab) that is allosterically regulated by cyclic nucleotide binding to a noncatalytic binding site (6). The PDE6 catalytic dimer has several features that distinguish it from all other PDE families: (1) the isoform of PDE6 in the rod photoreceptor is composed of two different catalytic subunits, α and β ($P\alpha\beta$), whereas cone PDE6 and the other ten families have two identical catalytic subunits; (2) cGMP hydrolysis catalyzed by $P\alpha\beta$ operates at a diffusion-controlled limit; (3) $P\alpha\beta$ catalytic activity is suppressed by several hundred-fold through the binding of two inhibitory γ-subunit ($P\gamma$) to form the PDE6 holoenzyme ($\alpha\beta\gamma\gamma$); (4) the activation of PDE6 holoenzyme results from $G\alpha_t$-induced displacement of $P\gamma$ from $P\alpha\beta$; (5) PDE6 is the only member of this enzyme superfamily that cannot be obtained in an active form from eukaryotic or prokaryotic heterologous expression systems (7).

In comparison to other PDE families, structural information about the molecular organization of PDE6 holoenzyme is limited. Crystal structures of the catalytic and tandem GAFab domains of PDE5 (the most closely related PDE family to PDE6) (8, 9) as well as a nearly full-length structure of the GAFab-containing PDE2 catalytic dimer (10) have been determined. In contrast, only the GAFa domain of cone PDE6 was determined at atomic resolution (11). Although the overall molecular organization of PDE6 holoenzyme was defined using negative-stain electron microscopy, the interface between catalytic and inhibitory subunits as well as the quaternary structure of $P\alpha\beta$ remain elusive (12, 13).

The regulatory Pγ subunit inhibits cGMP hydrolysis by direct binding of its last ten amino acid residues at the entrance to the active site (14–16). These biochemical studies are supported by a structure of the PDE5 catalytic domain, in which the M-loop and the α-helix 15 region in the PDE6 catalytic domain were substituted and the resulting chimera complexed with a C-terminal peptide of Pγ (17). Pγ also allosterically regulates the affinity of cGMP binding to the GAFa domain (18, 19), a function that has been localized to a region within the first third of the Pγ sequence (15, 20). Simultaneous interaction of this 87-residue polypeptide with the catalytic site and the GAFa domain suggests a highly extended conformation of Pγ consistent with chemical cross-linking/peptide mapping studies (21) but in marked contrast to the disordered structure of Pγ in solution (22). Furthermore, there is evidence that Pγ may form structurally and functionally distinct interactions with the α- and β-subunit (21, 23), however, little is known about the structural determinants that contribute to these different interactions.

Here, we utilize chemical cross-linking and mass spectrometric analysis (CXMS) to structurally characterize PDE6 holoenzyme. The CXMS approach can identify amino acid residues in spatial proximity but distant in primary sequence, providing intermediate resolution information on relative domain positions and orientations (24–27). In addition, CXMS data can be often complemented by other kinds of structural data, significantly improving the accuracy of resulting structural models (28). To this end, we have identified 43 intersubunit and 40 intrasubunit cross-linked pairs, followed by building a model of the PDE6 holoenzyme using an integrative modeling approach (29). The model defines the dimerization surfaces of the Pαβ catalytic heterodimer and maps binding sites of the inhibitory Pγ subunit on Pαβ, thus providing insight into the activation/deactivation cycle of PDE6.

Results

Cross-linking of PDE6 holoenzyme

We first assessed the cross-linking efficiency of various chemical reagents on PDE6 holoenzyme by monitoring cross-linked products on SDS-PAGE. For instance, when cross-linked with BS3 or Sulfo-MBS, PDE6 holoenzyme produced covalent complexes, migrating at ~110 kD (αγ βγ) and 200–250 kD (αβ, αβγ and αβγγ) in SDS gels (Fig. 1A). Both cross-linked and uncross-linked gel bands were excised and processed for in-gel digestion and mass spectrometric analysis to identify cross-linked peptides. To access surfaces of different physicochemical properties and generate a high-density cross-linking map of the PDE6 holoenzyme, we utilized multiple chemical cross-linkers of varying lengths and chemical functionalities. In addition, we included multiple proteases for sample digestion to improve the recovery and identification of cross-linked peptides. The short inhibitory γ-subunit is highly acidic in its C-terminal half, with no tryptic cleavage site from G46 to I87, which prevents the identification of cross-linked sites in this region even when using multiple proteases. Therefore, we engineered various mutants with trypsin cleavage sites in the C-terminal region of Pγ Only Pγ mutants with similar inhibition potency to that of the endogenous γ-subunit (Supplemental Table 1) were selected to reconstitute with the Pαβ

catalytic dimer. As expected, purified and reconstituted PDE6 holoenzymes (with either wild-type or mutant Pγ) behaved similarly in cross-linking reactions (Fig. 1A).

Collectively, we have identified 43 intersubunit and 40 intrasubunit cross-linked residue pairs (Table 1, 2 and 3). For most cross-links, the identification was based on multiple cross-linked peptides with different charge states, methionine oxidation states, and numbers of missed cleavage sites. This reproducible identification of the cross-linked peptides in our dataset suggests that we accurately mapped the native conformation of the PDE6 holoenzyme. A representative tandem MS spectrum of a cross-linked peptide is shown in Fig. 1B. The nearly complete sequence ion series (y and b ions) elucidate both the identity of two cross-linked peptides and the cross-linking site.

The catalytic subunits of the PDE6 holoenzyme, Pα and Pβ, are highly similar (72.6% sequence identity in bovine PDE6). Such high sequence identity results in additional complexity in cross-linking site assignment, because sequence information is sometimes insufficient on its own to distinguish intersubunit cross-links from intrasubunit cross-links. To reduce the ambiguity in cross-linked site assignment, we included cross-linked monomer samples (from the ~100 kD band) in analysis to distinguish intersubunit cross-links from intrasubunit cross-links. Using this approach, we were able to identify novel intersubunit interactions (27, 30), which were confirmed later by results from crystallography (31) or site-directed mutagenesis (27). Taking the aforementioned cross-linked peptide in Fig. 1B as an example, among the peptides that elute at ≈39.5 min from the reverse-phase capillary column, the peptide is present only in the digest of the ~220 kD Pαβγγ/Pαβγ band (Fig. 1C, at m/z 1004.21^{3+}). Extracted ion chromatograms (XIC) of this peptide further validate its absence in the monomer sample (Fig. 1C insets). Similar result was obtained in several other replicates. Since our cross-linking conditions didn't noticeably perturb the conformation of PDE6 holoenzyme, conformers in ~220 kD and ~100 kD bands should be indistinguishable. In addition, the high affinity between Pα and Pβ (existing as an obligatory dimer or in holoenzyme) preclude distinct monomeric conformers. Therefore, we assigned this peptide as an intersubunit cross-linked peptide.

Though only limited structural information on PDE6 is available, the crystal structure of the catalytic domain for a human cone PDE5/6 chimera has been determined (17). This chimera shares 49% sequence identity with the bovine PDE6 catalytic domains of the α- and β-subunit and is potently inhibited by the PDE6 inhibitory subunit, Pγ (17). Hence, we used it as a template to build models for the catalytic domains of bovine PDE6 α- and β-subunit with Modeller v9.11 (32). Except for an insertion of 8 amino acid residues (686–694 in Pβ), our top scored models for the catalytic domains of the α- and β-subunit highly resemble the chimera template (Fig. 1D). Five Pα and thirteen Pβ intrasubunit cross-links, as well as six intersubunit cross-links between Pγ and Pα or Pβ were localized to the region of the catalytic domains well aligned with the PDE5/PDE6 chimera structure. We inspected the Cα distances of cross-linked residues on our top scored models of the Pα and Pβ catalytic domains (Supplemental Table 2). The distances of all cross-linked Cα pairs were within the maximal extension of the corresponding cross-linkers. These results suggest that: (1) the PDE5/6 catalytic domain chimera structure is an accurate representation of the PDE6 catalytic domain inhibited by PDE6 γ-subunit; (2) the conformation of the PDE6

holoenzyme remained intact under our cross-linking conditions; (3) mutations introduced in Pγ did not noticeably alter the interactions of Pγ with the catalytic domains of the α- and β-subunit.

Parallel orientation of catalytic subunits in PDE6 holoenzyme

With the available domain structures of the PDE superfamily proteins (10, 11, 33), we examined the position of intersubunit cross-links between the α- and β-subunit. Many Pα and Pβ intersubunit cross-linked residues were localized to the extended α-helical regions of the GAFa and GAFb domains, such as Pβ K78, K391, K440 and Pα K247, K447. These cross-links suggested that the α-helical sides of the GAFa and GAFb domains interact to form part of the catalytic dimer interface, with allosteric cGMP binding sites in GAFa domains facing outward. Furthermore, many intersubunit cross-links were either between the GAFa domains of the α- and β-subunit or between the GAFb domains of the α- and β-subunit, supporting a parallel orientation between two catalytic subunits.

Together, our cross-linking data suggested a parallel dimer arrangement, with juxtaposed α-helices contributing to the contacts at the Pαβ dimer interface. A similar spatial organization of the Pαβ catalytic heterodimer was previously observed in the crystal structures of a nearly full-length, *apo*-state PDE2 catalytic dimer (10), and a PDE5 tandem GAFa/b dimer (9). The dimer arrangement is also consistent with a previous biochemical study to determine the heterodimerization interface of the α- and β-subunit (34). In contrast, the parallel arrangement with long interacting α-helices is different from an anti-parallel domain orientation observed in the crystal structure of a PDE5 GAFb dimer (33), as well as from a domain-swapping conformation observed in the crystal structure of a cGMP-bound PDE2 GAFab dimer (35).

Although the organization of the GAFab domains in the *apo* PDE2 catalytic dimer structure is in good agreement with our data, an αβ intersubunit cross-link between Pα K447 and Pβ K618 suggests a different arrangement for the catalytic domains of the Pαβ heterodimer. Pβ K618 resides in the H-loop near the catalytic site. In the crystal structure of *apo* PDE2 catalytic dimer (10), the H-loop from each catalytic subunit packs tightly against the catalytic site, meanwhile contributing to the contacts at the heterodimer interface (Fig. 2A). In this ‘closed’ conformation, Pβ K618 is buried in the heterodimer interface, thus, is not available to form the cross-link with Pα K447 on the linker region between the GAFb domain and the catalytic domain. Therefore, our data suggest an ‘open’ conformation, where the two catalytic domains of Pα and Pβ swing away from the heterodimer interface.

Pαβ catalytic dimer modeling

To gain further insights into the subunit arrangement in PDE6 holoenzyme, we have built a set of models for the Pαβ catalytic dimer with an integrative modeling approach (29, 36).

Comparative models based on multiple templates (PDE2, PDE5/6 chimera and PDE6 for the overall structure, catalytic domain and GAFa domain, respectively) were built with Modeller v9.11. The resulting models satisfied all but one cross-link when setting an upper bound threshold on the Cα-Cα distance to 19.8 Å, 27.4 Å, 37.7 Å and 51.8 Å for Sulfo-MBS, DSS,

BS(PEG)5 and BS(PEG)9, respectively. The upper bound was computed using the maximal extension of the cross-linker, the cross-linked residues and an additional 1.5 Å for estimated coordinate error. The unsatisfied BS(PEG)9 cross-link was between Pα 613 and Pβ 315 with the Cα-Cα distance of 58.7 Å. The Cα atoms of four cross-linked pairs were within 2 Å of the upper bound: Pα 31 and Pβ 78; Pα 21 and Pβ 78; Pα 393 and Pα 620 (or Pβ 391 and Pβ 618). The H-loop region could not be easily modeled without steric clashes (Fig. 2A, colored in green), when individual catalytic domains (modeled from the PDE5/6 chimera structure) were modeled into the PDE2 template. Such clashes are largely due to a unique position of the H-loop in the PDE2 template, which allows an extensive dimerization of the two catalytic domains in the *apo* PDE2 structure (10). The C-terminal segment of Pγ in the PDE5/6 chimera template displaces the H-loop (17) and pushes it towards the dimer interface, which causes steric clashes in our models. Moreover, the models did not fit well into a previously published EM density map (Fig. 2A) (12). These results suggested that the relative positions and orientations of the catalytic domains are different from those in the comparative models.

Hence, we further improved the comparative models by incorporating other available knowledge about PDE6 using our open-source *Integrative Modeling Platform* software (IPM; http://integrativemodelling.org) (29, 37). Our cross-links, the EM density map (12) and related template structures were translated into spatial restraints on PDE6, followed by conformational sampling in the search for models that satisfy these restraints (Material and Methods). The approach resolved the steric clashes by exposing H-loops, improved cross-linking scores and the fit to the EM density map (Fig. 2B). The 100 best scoring models cluster into two major groups, named clusters 1 and 2, with 63 and 37 members, respectively. The precision, calculated as the average Cα-RMSD between each pair of cluster members, is approximately 7.8 and 5.0 Å for clusters 1 and 2, respectively. The structures in the two clusters have a similar organization of the GAFab domains, while they differ in the orientations of the catalytic domains (Fig. 2B, Fig. S2). Cluster 1 (Fig. 2B) has the catalytic domains swapped with respect to the GAF domains, as observed in the PDE2 crystal structure, while cluster 2 does not display domain swapping (Fig. S2). All models satisfy the input restraints approximately equally well and cannot be discriminated based on the existing data. The EM cross-correlation coefficient improved from 0.63 for the initial comparative model to 0.70 for cluster 1 and 0.69 for cluster 2. The two clusters are in excellent agreement with cross-linking data: all Cα-Cα distances for all cross-linked pairs are well below the estimated upper bound on the distance. However, in cluster 2, the conformation of the 300–340 loop in both subunits is implausibly extended towards the opposite subunit to satisfy the Pα 613 and Pβ 315 cross-link. Therefore, we suggest that cluster 1 represents the more likely PDE6 conformation.

Asymmetric cross-linking of inhibitory Pγ subunit in PDE6 holoenzyme

Besides cross-links along the catalytic dimer interface, we identified additional cross-linked pairs between the inhibitory γ-subunits and the αβ catalytic dimer (Table 3). The cross-link between Pγ K25 and Pα C163 suggests a spatial proximity between the N-terminal polycationic region of Pγ and the GAFa domain of Pα (Fig. 3A). Pα C163 is next to the short H4 ‘lid’-helix, right above the noncatalytic cGMP binding pocket (9). Moreover, Pα

C163 is in vicinity to a highly conserved surface composed of numerous negatively charged and hydrophobic residues (11), likely interacting with the polycationic region of Pγ

In the β-subunit, a cysteine residue (C157) also exists in the 'lid' region of a noncatalytic cGMP binding site, nearly symmetric to C163 in Pα (Fig. 3B). Despite the identification of the Pα C163 cross-link in multiple samples, we never detected the corresponding Pβ C157 cross-link. The reason was not difficult peptide detection, because the unmodified peptide in this region of Pβ was consistently observed with comparable mass and good ion intensity (Fig. 3C).

A likely reason is a significantly lower cross-linking yield between Pβ and Pγ in the 'lid' region of the noncatalytic cGMP binding pocket. To investigate this possibility, we used a semi-quantitative, spectral counting approach to estimate the amount of Pα and Pβ in the Sulfo-MBS cross-linked ~110 kD band samples (38, 39). We observed a nearly 2-fold reduction of Pβ in the cross-linked Pαγ or Pβγ dimer mixture migrating at 110 kD, along with a substantial increase of Pβ in the 100 kD region of Pα or Pβ mixture (Fig. 3D). Such depletion of Pβ in the Pαγ or Pβγ cross-linked dimer was specific to Sulfo-MBS cross-linking, because a similar amount of Pα and Pβ was detected in the Pαγ or Pβγ dimer when DSS was used as the cross-linker. DSS cross-linked Pγ to Pα and Pβ at multiple sites, without appreciable preference for overall cross-linking yield. Therefore, a depletion of Pβ in the Sulfo-MBS cross-linked Pαγ or Pβγ dimer implicated a Pγ binding discrepancy between Pα and Pβ at the noncatalytic cGMP binding site.

Such α- and β-subunit preference in cross-linking around the noncatalytic cGMP pocket was indicative of a substantial sequence divergence between two catalytic subunits in the 'lid' region, despite a >72% overall sequence identity (Fig. 3B). To examine the possibility of an asymmetric binding of the γ subunit to the α- and β-subunit around the noncatalytic cGMP pocket in the GAFa domain, we explored additional possible contacts by introducing a photoactivatable benzoylphenylalanine (Bpa) mutation at amino acid residue 23 of the Pγ sequence (40). The benzophenone functional group can react with any amino acid residue that is close in space, and is thus less sensitive to the orientation of side-chains. Using mass spectrometric analysis, we detected a high abundance cross-linked peptide in the digest of the cross-linked 110 kD gel band, with Pγ Bpa23 cross-linked to Pα F165 or V166 (Fig. 4A). In a previous study, the Pγ Bpa23 cross-linking site was identified as Pα M138 or G139 using a biotinylated Pγ 21–45 peptide (41). Our LC-MS/MS analysis detected the unmodified M138/G139-containing peptide, but not the cross-linked peptide. The discrepancy in the site of Pα cross-linking is likely due to the differences in the binding of full-length Pγ (this study) versus the Pγ 21–45 peptide used by Muradov *et al.* (41). However, the M138/G139-segment and the F165/V166-segment are in spatial proximity, according to the crystal structure of the cone PDE6 GAFa domain (11). Consistent with the Sulfo-MBS cross-linking results, we observed a similar ~2-fold depletion in β subunit cross-linking, when compared to the 100 kD and 110 kD controls with the spectral counting method (Fig. 4B).

Although the 'lid' region of Pβ does not cross-link effectively to the GAF-interacting region of Pγ (I10-K45), two residues flanking this region (E156 and D169) were cross-linked to K7

of Pγ by EDC, a zero-length cross-linker. However, the spatial distance between these two residues in the GAFa structure of cone PDE6 is too large for both of them to be cross-linked to Pγ K7 by a zero-length cross-linker. Therefore, while interacting with Pβ the N-terminal tail of Pγ is likely mobile, adapting multiple positions in space. In agreement, Pγ K7 is also cross-linked to Pβ K78 near the dimer interface in the DSS cross-linking samples.

Despite two EDC cross-linked pairs between Pβ and Pγ we have not detected any EDC cross-link between Pα and Pγ even though both acidic cross-linking sites are conserved in Pα. To determine whether there was any preference towards Pβ in EDC cross-linking, we carried out spectral counting quantitation for the EDC cross-linked samples (Fig. 3D). A noticeable enrichment of Pβ was detected in the cross-linked 110 kD gel band, with substantial reduction of Pβ in the 100 kD gel band. In summary, our data strongly suggest an asymmetric binding of the γ subunit to the α- and β-subunit around the noncatalytic cGMP binding site.

We also applied the benzophenone cross-linking strategy to other Pγ residues. We introduced several Cys mutants, which were subsequently labeled with MBP (4-(N-maleimido)benzophenone), to investigate potential binding differences between the α- and β-subunit to various regions of the γ subunit (Fig. 4B). No appreciable cross-linking difference between the α- and β-subunit was detected for the Pγ C-terminal region (C73-MBP and C84-MBP), consistent with a previous study (42). Moreover, we detected a substantial higher Pβ cross-linking yield for the Pγ C30-MBP mutant, contradicting a previous radiolabel transfer study where a higher Pα cross-linking efficiency was reported for Pγ at position 30 (23). This discrepancy in cross-linking preference could have resulted from the difference in cross-linking probes utilized in these two studies. Our labeling probe was significantly shorter than the probe used in the label-transfer study. In order for the length of labeling probes to affect cross-linking preference, residue Pγ C30 needs to reside near the dimeric interface of the Pαβ catalytic dimer.

Discussion

Rod PDE6 is the only effector enzyme of the 11-member phosphodiesterase superfamily that consists of two different catalytic subunits forming a heterodimer, Pαβ, which is regulated by two identical inhibitory Pγ subunits. Tangible progress has been made in determining atomic structures of several individual domains and low-resolution topological organization of the PDE6 holoenzyme (11–13, 17). However, a more detailed structure of the entire PDE6 remains lacking. Challenges include obtaining a sufficient amount of protein from ROS membrane preparation and recombinant expression of PDE6.

In this study, we used chemical crosslinking and mass spectrometric analysis to generate a high-density cross-linking map of surface residues from various subunits and domains of the PDE6 holoenzyme. Our results are in excellent agreement with several high-resolution structures for individual domains of phosphodiesterase superfamily enzymes, supporting the biochemical and functional relevance of our data. For instance, the consistency between our results and the crystal structure of the chimeric PDE5/6 catalytic domain mutually validates these two studies. In addition, the intersubunit cross-links between the GAFab domains of

the α- and β-subunit support a parallel orientation of the Pαβ heterodimer with juxtaposed α-helices forming the dimeric interface, as observed in crystal structures of *apo* PDE2 (10) and the PDE5 GAFab tandem dimer (9). We built a model of the PDE6 holoenzyme by satisfying spatial restraints implied by cross-links, related crystallographic structures and an EM density map. The model describes the architecture of the holoenzyme and interacting surfaces between the subunits, thus providing structural insights into the catalysis and regulation of the PDE6 holoenzyme.

Architecture of PDE6 holoenzyme

In our model, the Pαβ catalytic dimer adopts an overall domain arrangement similar to the *apo*-structure of the PDE2 homodimer (10). However, the two catalytic domains in our model swing away from the dimer interface and rotate clockwise for about 90°, placing the catalytic sites on two solvent-accessible, opposite sides (Fig. 5). This ‘open’ configuration, with two catalytic sites on opposite sides of the catalytic dimer, has significant functional implications for the activation/deactivation cycle of the PDE6 holoenzyme, intricately regulated by the inhibitory γ-subunit and transducin.

The displacement of inhibitory Pγ activates PDE6 to be a “perfect” enzyme, with a diffusion-controlled catalysis rate. In addition, no extensive conformational change between Pαβ and the PDE6 holoenzyme has been detected by analytical ultracentrifugation (43). Our model suggests a conformation in which PDE6 becomes fully active upon Pγ removal, without extensive domain rearrangements implicated in other PDE families. Secondly, our model points to a region on the Pαβ catalytic dimer (Fig. 5, red asterisk) that provides a high affinity docking site for the middle section of Pγ (15). The position of this Pγ-interacting region in Pαβ is consistent with the putative location of the Pγ subunit in the 18 Å EM map of PDE6 (12). The middle section of Pγ also interacts with transducin G_{α}· GTPγS, forming a secondary interaction site complementary to the interaction site around the Pαβ catalytic site (15, 44). The close vicinity of these two sites in our model suggests a concerted binding of activated transducin G_{α}· GTPγS to the PDE6 holoenzyme upon activation.

Moreover, the positions of the Pαβ residues cross-linked to Pγ (Fig. 5, magenta dots) delineate an extended, near 2-fold symmetry binding mode of Pγ in the PDE6 holoenzyme. Except for the N-terminal 25 residues and the C-terminal tail, most of the Pγ middle section docks near the dimer interface of the Pαβ heterodimer in our models. This Pγ binding geometry might be the underlying reason for a previously observed simultaneous binding of each γ-subunit to both the α- and β-subunit (21, 23). Interesting, several deleterious missense mutations, such as Pα R102C (45), Pβ H258N (46) and cone PDE6 M455V (47), are localized in close proximity to residues that are cross-linked to Pγ in the model. Therefore, these mutations likely affect vision by interfering with the proper binding of Pγ In addition, our model suggests potentially two non-exclusive binding sites for transducin on the PDE6 central effector enzyme (48).

Asymmetric interaction of the γ-subunit with the GAFa domains of Pα and Pβ

In addition to being the substrate of PDE6, cGMP binds to a noncatalytic site in each GAFa domain of the PDE6 catalytic dimer. The GAFa domain also interacts with the inhibitory γ-

subunit. The interactions of Pγ and noncatalytic cGMP with the GAFa domain act in a synergistic manner, with Pγ enhancing the noncatalytic cGMP binding and *vice versa* (49). Therefore, this reciprocal binding relationship in the GAFa domain provides additional opportunity to regulate the cytoplasmic cGMP concentration and the activation window of PDE6 during phototransduction (50). In addition, the two noncatalytic cGMP binding sites display different affinity towards cGMP (49). However, it remains unknown whether or not this difference in cGMP affinity stems from intrinsic differences in the GAFa domains of the α- and β-subunit. It is also not clear which catalytic subunit preferentially interacts with noncatalytic cGMP.

Our study elucidates two different binding modes of Pγ at the 'lid' region of noncatalytic cGMP sites in the GAFa domains of the α- and β-subunit. Though cross-links around the 'lid' regions of both catalytic subunits have been identified, the K25 region of Pγ interacts with the α-subunit while the N-terminal region of Pγ interacts with the β-subunit. Since the N-terminal tail of Pγ seems to be mobile and cross-links to several distinct sites of the β-subunit, it is tempting to speculate that the interaction between the γ-and β-subunit exists in a less-defined, thus low-affinity state in this region compared to that of the α-subunit. Conversely, the high affinity binding of Pγ to the α-subunit in the GAFa domain might provide a mechanism for a rapid deactivation of rod PDE6 upon $G\alpha_t$ hydrolysis. Consistent with this idea, ectopic expression of cone PDE6 (which has higher sequence similarity to the β-subunit than the α-subunit) in rod photoreceptors led to nearly two-fold slower deactivation in light responses (51). This asymmetric binding of the inhibitory γ-subunit around the noncatalytic cGMP binding sites in the two GAFa domains of Pαβ likely underlies the previously observed heterogeneity in cGMP binding to Pαβ. Conceivably, this Pγ-regulated asymmetry in cGMP binding may fine-tune the nonactivated and transducin-activated states of each catalytic subunit, broadening the feedback control these noncatalytic cGMP binding sites have rod PDE6 holoenzyme.

Material and Methods

Materials

Bovine retinas were purchased from W. L. Lawson, Inc. For the preparation of wild-type and mutant Pγ, primers from Invitrogen, plasmid purification kits from Qiagen and QuikChange mutagenesis kit fom Agilent Technologies were used. Proteolytic enzymes were purchased from Promega (trypsin and chymotrypsin) or Roche (Glu-C and Lys-C). Except for MBP (4-(N-Maleimido) benzophenone) (Sigma), chemical cross-linkers were purchased from Pierce, including DSS (disuccinimidyl suberate), BS3 (Bis(sulfosuccinimidyl)suberate), BS(PEG)5 (Bis(succinimidyl) penta(ethylene glycol)), BS(PEG)9 (Bis(succinimidyl) nona(ethylene glycol)), EDC (1-Ethyl-3-(3-dimethylaminopropyl)carbodiimide) and Sulfo-MBS (m-maleimidobenzoyl-N-hydroxysulfosuccinimide ester).

Protein preparation

PDE6 holoenzyme and Pαβ catalytic dimer were prepared as described previously (7). Site-directed mutagenesis of Pγ was carried out using pET11a-Pγ 1–87 plasmid as template, and

mutants were expressed in *E. coil* BL21/DE3 cells, purified through SP-Sepharose column and reverse-phase chromatography (15). To make Pγ single Cys mutants for MBP cross-linking, the native Cys68 was also substituted with Ser. MBP labeling was carried out by incubating 200 μM Pγ (containing a single Cys) with a 20-fold excess of MBP at RT for 1hr, quenched with 200 mM DTT in 100 mM Tris before HPLC purification (21). To prepare *p*-benzoyl-L-phenylalanine (Bpa) incorporated Pγ 23Bpa, the codon for 23Pro was mutated to an amber stop codon (TAG), and the construct was co-transformed with the pEVOL-pBpF plasmid (from Addgene) to BL21/DE3 cells as described previously (40). For the reconstitution of PDE6 holoenzyme, purified Pαβ (0.2 nM–1nM) was pre-incubated with purified Pγ at room temperature for 20 min, followed by adding 2 mM cGMP. The catalytic activity of reconstituted PDE6 was measured by the phosphate release assay (52). The inhibition potency (IC_{50}) was calculated from curve fitting the results to a 3-parameter logistic equation.

Chemical cross-linking, in-gel digestion and mass spectrometric analysis

Chemical cross-linking reactions were carried out, following the Pierce instruction for each cross-linker. PDE6 holoenzyme was buffer-exchanged into either HEPES buffer (20 mM HEPES, 100 mM NaCl, 5mM $MgCl_2$, pH 8.0) for BS3, DSS, BS(PEG)5, BS(PEG)9 and Sulfo-MBS cross-linking; or MES buffer (100 mM MES, pH 6.5) for EDC cross-linking. The PDE6 holoenzyme was cross-linked with ~50-fold molar excess of the cross-linker. After the cross-linking reaction was quenched, proteins were precipitated with trichloroacetic acid, separated by SDS-PAGE and visualized with Coomassie brilliant blue G-250.

Cross-linked products were in-gel digested and analyzed by LC-MS and LC-MS-MS as described previously (53). Briefly, l μ1 aliquot of the digestion mixture was injected into an Dionex Ultimate 3000 RSLCnano UHPLC system (Dionex Corporation, Sunnyvale, CA), and separated by a 75 μm × 25 cm PepMap RSLC column (100 Å, 2 μm) at a flow rate of ~450 nl/min. The eluant was connected directly to a nanoelectrospray ionization source of an LTQ Orbitrap XL mass spectrometer (Thermo Scientific, Waltham, MA). LC-MS data were acquired in an information-dependent acquisition mode, cycling between a MS scan (m/z 315-2,000) acquired in the Orbitrap, followed by low-energy CID analysis on 3 most intense multiply charged precursors acquired in the linear ion trap.

Cross-linked peptide identification

Cross-linked peptides were identified using an integrated module in Protein Prospector, based on a bioinformatic strategy described previously (54, 55). The score of a cross-linked peptide was based on number and types of fragment ions identified, as well as the sequence and charge state of the cross-linked peptide. Only results where the score difference is greater than 0 (i.e. the cross-linked peptide match was better than a single peptide match alone) are considered. The expectation values are calculated based on matches to single peptides, so should be treated as another score, rather than a statistical measure of reliability.

Comparative modeling

Comparative modeling with Modeller v9.11 (32) relied on an alignment of the target sequence with multiple template structures: near full-length PDE2 dimer (PDB: 3IBJ), PDE5 catalytic domain (PDB: 3BJC, 3JWR, 1TBF), and PDE6 GAFa domain (PDB: 3DBA). Multiple sequence alignment of PDE6 and template structures was obtained using HHpred (56). To enforce the symmetry of the complex observed in the crystal structures of the templates, a "DRMS" restraint was added between Cα atoms of corresponding residues of the two chains. In the PDE6 regions without a template, α-helical secondary structure was imposed on the segments consistently predicted as α-helices by secondary structure prediction methods implemented in the Quick2D webserver. The comparative model with the lowest DOPE score (57) out of 10 models was selected as an input for the integrative modeling protocol described below.

Integrative modeling

The input data files, modeling scripts and output models can be downloaded from http://salilab.org/pde6. Each residue in the comparative model was represented by a single bead centered on its Cα atom. Each chain in the dimer was divided into 6 rigid bodies, corresponding to residue ranges 1–69 (N-terminal region), 70–204 (N-terminal portion of GAFa), 205–251 (C-terminal helix of GAFa), 252–413 (N-terminal portion of GAFb), 414–453 (C-terminal helix of GAFb) and 454–814 (catalytic domain). The disordered C-terminal region 814–859 was excluded from the model. The scoring function consisted of 6 types of a term. First, to maintain sequence connectivity, a harmonic restraint was added between the C-terminal and N-terminal residues of two consecutive rigid bodies. Second, a cross-link was encoded by a harmonic restraint between the Cα atoms of cross-linked residues with a mean distance of 12 Å and a standard deviation of 5 Å for the BS3 and DSS cross-linkers (58). For Sulfo-MBS, BS(PEG)5 and BS(PEG)9, the mean distance of 10.0 Å, 19.2 Å and 26.4 Å, and the standard deviation of 3.6 Å, 6.8 Å and 9.4 Å, was imposed respectively. To improve numerical stability of conformational sampling, the harmonic restraint was truncated at a distance larger than 13, 15, 24 and 35 Å for the Sulfo-MBS, BS3/DSS, BS(PEG)5 and BS(PEG)9 cross-linkers. Third, the EM score was computed by fitting a model into the EM density map using principal component analysis (28). Fourth, to encode template structure information for the GAFab domains, a harmonic distance restraint was imposed on residue pairs in distinct rigid bodies with a distance lower than 6.5Å. The distance corresponding to the minimum of the harmonic restraint was derived from the initial comparative model, and the force constant was set to 1.0. Fifth, the excluded volume between rigid bodies was modeled by a pairwise soft-sphere repulsive potential, where the volume of each Cα bead equals the volume of the corresponding amino acid residue (59). Finally, to reduce the search space, a C2 symmetry constraint was added between equivalent rigid bodies of the two PDE6 chains. We heuristically set the weights of the EM and the cross-link score terms to 5.0 and 0.5, respectively; others were set to 1.0. 10^4 models were generated using Metropolis Monte-Carlo sampling enhanced by simulated annealing with high and low temperatures set to 0.5 and 2.0, respectively. At each sampling step, a new system configuration was produced by randomly translating and rotating a single rigid body by a random value. A total of 6×10^6 sampling steps were performed. All atom models were generated from the 10 best scoring coarse-grained models and refined as follows. First,

backbone atoms and side-chains were threaded on the Cα atom positions using Pulchra (60). Second, these models were refined using Modeller v9.11 that also modeled the missing regions of the proteins using cross-linking data as restraints.

Supplementary Material

Refer to Web version on PubMed Central for supplementary material.

Acknowledgments

We thank David Lodowski and Krzysztof Palczewski for providing the EM density map (12), Peter Baker and Al Burlingame for access to a developmental version of the Protein Prospector software, Ben Webb and Maya Topf for help with Modeller. This work was supported by NSF CLF 1307367, NIFA/USDA H00567 and UNH Karabelis Fund (to FC), NIH EY-05798 (to RHC), NIH NIGMS R01 GM083960 and U54 RR022220 (to AS), NIH NIGMS 8P41GM103481 (RJC). RP was supported by Swiss National Science Foundation grants PA00P3-139727 and PBZHP3-133388.

References

1. Palczewski K, Orban T. From atomic structures to neuronal functions of g protein-coupled receptors. Annu Rev Neurosci. 2013; 36:139–164. [PubMed: 23682660]
2. Wensel TG. Signal transducing membrane complexes of photoreceptor outer segments. Vision Res. 2008; 48(20):2052–2061. [PubMed: 18456304]
3. Arshavsky VY, Burns ME. Photoreceptor signaling: supporting vision across a wide range of light intensities. J Biol Chem. 2012; 287(3):1620–1626. [PubMed: 22074925]
4. Daiger SP, Sullivan LS, Bowne SJ. Genes and mutations causing retinitis pigmentosa. Clin Genet. 2013; 84(2):132–141. [PubMed: 23701314]
5. Conti M, Beavo J. Biochemistry and physiology of cyclic nucleotide phosphodiesterases: essential components in cyclic nucleotide signaling. Annu Rev Biochem. 2007; 76:481–511. [PubMed: 17376027]
6. Zoraghi R, Corbin JD, Francis SH. Properties and functions of GAF domains in cyclic nucleotide phosphodiesterases and other proteins. Mol Pharmacol. 2004; 65(2):267–278. [PubMed: 14742667]
7. Pentia DC, Hosier S, Collupy RA, Valeriani BA, Cote RH. Purification of PDE6 isozymes from mammalian retina. Methods Mol Biol. 2005; 307:125–140. [PubMed: 15988060]
8. Wang H, et al. Multiple conformations of phosphodiesterase-5: implications for enzyme function and drug development. J Biol Chem. 2006; 281(30):21469–21479. [PubMed: 16735511]
9. Wang H, Robinson H, Ke H. Conformation changes, N-terminal involvement, and cGMP signal relay in the phosphodiesterase-5 GAF domain. J Biol Chem. 2010; 285(49):38149–38156. [PubMed: 20861010]
10. Pandit J, Forman MD, Fennell KF, Dillman KS, Menniti FS. Mechanism for the allosteric regulation of phosphodiesterase 2A deduced from the X-ray structure of a near full-length construct. Proc Natl Acad Sci U S A. 2009; 106(43):18225–18230. [PubMed: 19828435]
11. Martinez SE, Heikaus CC, Klevit RE, Beavo JA. The structure of the GAF A domain from phosphodiesterase 6C reveals determinants of cGMP binding, a conserved binding surface, and a large cGMP-dependent conformational change. J Biol Chem. 2008; 283(38):25913–25919. [PubMed: 18614542]
12. Goc A, et al. Structural characterization of the rod cGMP phosphodiesterase 6. J Mol Biol. 2010; 401(3):363–373. [PubMed: 20600113]
13. Kameni Tcheudji JF, et al. Molecular organization of bovine rod cGMP-phosphodiesterase 6. J Mol Biol. 2001; 310(4):781–791. [PubMed: 11453687]
14. Granovsky AE, Natochin M, Artemyev NO. The gamma subunit of rod cGMP-phosphodiesterase blocks the enzyme catalytic site. J Biol Chem. 1997; 272(18):11686–11689. [PubMed: 9115217]

15. Zhang XJ, Gao XZ, Yao W, Cote RH. Functional mapping of interacting regions of the photoreceptor phosphodiesterase (PDE6) gamma-subunit with PDE6 catalytic dimer, transducin, and regulator of G-protein signaling9–1 (RGS9–1). J Biol Chem. 2012; 287(31):26312–26320. [PubMed: 22665478]
16. Zhang Z, Artemyev NO. Determinants for phosphodiesterase 6 inhibition by its gamma-subunit. Biochemistry. 2010; 49(18):3862–3867. [PubMed: 20397626]
17. Barren B, et al. Structural basis of phosphodiesterase 6 inhibition by the C-terminal region of the gamma-subunit. Embo J. 2009; 28(22):3613–3622. [PubMed: 19798052]
18. Cote RH, Bownds MD, Arshavsky VY. cGMP binding sites on photoreceptor phosphodiesterase: role in feedback regulation of visual transduction. Proc Natl Acad Sci U S A. 1994; 91(11):4845–4849. [PubMed: 8197145]
19. Yamazaki A, Bartucca F, Ting A, Bitensky MW. Reciprocal effects of an inhibitory factor on catalytic activity and noncatalytic cGMP binding sites of rod phosphodiesterase. Proc Natl Acad Sci U S A. 1982; 79(12):3702–3706. [PubMed: 6285360]
20. Artemyev NO, Hamm HE. Two-site high-affinity interaction between inhibitory and catalytic subunits of rod cyclic GMP phosphodiesterase. Biochem J. 1992; 283 (Pt 1):273–279. [PubMed: 1314566]
21. Guo LW, et al. The inhibitory gamma subunit of the rod cGMP phosphodiesterase binds the catalytic subunits in an extended linear structure. J Biol Chem. 2006; 281(22):15412–15422. [PubMed: 16595671]
22. Song J, et al. Intrinsically disordered gamma-subunit of cGMP phosphodiesterase encodes functionally relevant transient secondary and tertiary structure. Proc Natl Acad Sci U S A. 2008; 105(5):1505–1510. [PubMed: 18230733]
23. Guo LW, et al. Asymmetric interaction between rod cyclic GMP phosphodiesterase gamma subunits and alphabeta subunits. J Biol Chem. 2005; 280(13):12585–12592. [PubMed: 15668239]
24. Rappsilber J. The beginning of a beautiful friendship: cross-linking/mass spectrometry and modelling of proteins and multi-protein complexes. J Struct Biol. 2011; 173(3):530–540. [PubMed: 21029779]
25. Singh P, Panchaud A, Goodlett DR. Chemical cross-linking and mass spectrometry as a low-resolution protein structure determination technique. Anal Chem. 2010; 82(7):2636–2642. [PubMed: 20210330]
26. Chu F, et al. Unraveling the interface of signal recognition particle and its receptor by using chemical cross-linking and tandem mass spectrometry. Proc Natl Acad Sci U S A. 2004; 101(47): 16454–16459. [PubMed: 15546976]
27. Wu B, et al. Structural basis for dsRNA recognition, filament formation, and antiviral signal activation by MDA5. Cell. 2013; 152(1–2):276–289. [PubMed: 23273991]
28. Schneidman-Duhovny D, et al. A method for integrative structure determination of protein-protein complexes. Bioinformatics. 2012; 28(24):3282–3289. [PubMed: 23093611]
29. Russel D, et al. Putting the pieces together: integrative modeling platform software for structure determination of macromolecular assemblies. PLoS Biol. 2012; 10(1):e1001244. [PubMed: 22272186]
30. Chu F, Maynard JC, Chiosis G, Nicchitta CV, Burlingame AL. Identification of novel quaternary domain interactions in the Hsp90 chaperone, GRP94. Protein Sci. 2006; 15(6):1260–1269. [PubMed: 16731965]
31. Shiau AK, Harris SF, Southworth DR, Agard DA. Structural Analysis of E. coli hsp90 reveals dramatic nucleotide-dependent conformational rearrangements. Cell. 2006; 127(2):329–340. [PubMed: 17055434]
32. Sali A, Blundell TL. Comparative protein modelling by satisfaction of spatial restraints. J Mol Biol. 1993; 234(3):779–815. [PubMed: 8254673]
33. Russwurm M, Schlicker C, Weyand M, Koesling D, Steegborn C. Crystal structure of the GAF-B domain from human phosphodiesterase 5. Proteins. 2011; 79(5):1682–1687. [PubMed: 21425347]
34. Muradov KG, Boyd KK, Martinez SE, Beavo JA, Artemyev NO. The GAFa domains of rod cGMP-phosphodiesterase 6 determine the selectivity of the enzyme dimerization. J Biol Chem. 2003; 278(12):10594–10601. [PubMed: 12531898]

35. Martinez SE, et al. The two GAF domains in phosphodiesterase 2A have distinct roles in dimerization and in cGMP binding. Proc Natl Acad Sci U S A. 2002; 99(20):13260–13265. [PubMed: 12271124]
36. Schneidman-Duhovny D, et al. A method for integrative structure determination of protein-protein complexes. Bioinformatics. 2012; 28(24):3282–3289. [PubMed: 23093611]
37. Alber F, et al. Determining the architectures of macromolecular assemblies. Nature. 2007; 450(7170):683–694. [PubMed: 18046405]
38. Zybailov B, Coleman MK, Florens L, Washburn MP. Correlation of relative abundance ratios derived from peptide ion chromatograms and spectrum counting for quantitative proteomic analysis using stable isotope labeling. Anal Chem. 2005; 77(19):6218–6224. [PubMed: 16194081]
39. Brickner DG, et al. Transcription factor binding to a DNA zip code controls interchromosomal clustering at the nuclear periphery. Dev Cell. 2012; 22(6):1234–1246. [PubMed: 22579222]
40. Chin JW, Martin AB, King DS, Wang L, Schultz PG. Addition of a photocrosslinking amino acid to the genetic code of Escherichiacoli. Proc Natl Acad Sci U S A. 2002; 99(17):11020–11024. [PubMed: 12154230]
41. Muradov KG, Granovsky AE, Schey KL, Artemyev NO. Direct interaction of the inhibitory gamma-subunit of Rod cGMP phosphodiesterase (PDE6) with the PDE6 GAFa domains. Biochemistry. 2002; 41(12):3884–3890. [PubMed: 11900530]
42. Artemyev NO, Natochin M, Busman M, Schey KL, Hamm HE. Mechanism of photoreceptor cGMP phosphodiesterase inhibition by its gamma-subunits. Proc Natl Acad Sci U S A. 1996; 93(11):5407–5412. [PubMed: 8643588]
43. Matte SL, Laue TM, Cote RH. Characterization of conformational changes and protein-protein interactions of rod photoreceptor phosphodiesterase (PDE6). J Biol Chem. 2012; 287(24):20111–20121. [PubMed: 22514270]
44. Guo LW, Hajipour AR, Ruoho AE. Complementary interactions of the rod PDE6 inhibitory subunit with the catalytic subunits and transducin. J Biol Chem. 2010; 285(20):15209–15219. [PubMed: 20231289]
45. Tsang SH, et al. A novel mutation and phenotypes in phosphodiesterase 6 deficiency. Am J Ophthalmol. 2008; 146(5):780–788. [PubMed: 18723146]
46. Gal A, Orth U, Baehr W, Schwinger E, Rosenberg T. Heterozygous missense mutation in the rod cGMP phosphodiesterase beta-subunit gene in autosomal dominant stationary night blindness. Nat Genet. 1994; 7(1):64–68. [PubMed: 8075643]
47. Thiadens AA, et al. Homozygosity mapping reveals PDE6C mutations in patients with early-onset cone photoreceptor disorders. Am J Hum Genet. 2009; 85(2):240–247. [PubMed: 19615668]
48. Clerc A, Catty P, Bennett N. Interaction between cGMP-phosphodiesterase and transducin alpha-subunit in retinal rods. A cross-linking study. J Biol Chem. 1992; 267(28):19948–19953. [PubMed: 1328188]
49. Mou H, Grazio HJ 3rd, Cook TA, Beavo JA, Cote RH. cGMP binding to noncatalytic sites on mammalian rod photoreceptor phosphodiesterase is regulated by binding of its gamma and delta subunits. J Biol Chem. 1999; 274(26):18813–18820. [PubMed: 10373499]
50. Zhang X, Cote RH. cGMP signaling in vertebrate retinal photoreceptor cells. Front Biosci. 2005; 10:1191–1204. [PubMed: 15769618]
51. Deng WT, et al. Cone phosphodiesterase-6alpha' restores rod function and confers distinct physiological properties in the rod phosphodiesterase-6beta-deficient rd10 mouse. J Neurosci. 2013; 33(29):11745–11753. [PubMed: 23864662]
52. Cote RH. Kinetics and regulation of cGMP binding to noncatalytic binding sites on photoreceptor phosphodiestrase. Methods Enzymol. 2000; 315:646–672. [PubMed: 10736732]
53. Chu F, et al. Unraveling the interface of signal recognition particle and its receptor by using chemical cross-linking and tandem mass spectrometry. Proc Natl Acad Sci U S A. 2004; 101:16454–16459. [PubMed: 15546976]
54. Chu F, Baker PR, Burlingame AL, Chalkley RJ. Finding chimeras: a bioinformatics strategy for identification of cross-linked peptides. Mol Cell Proteomics. 2010; 9(1):25–31. [PubMed: 19809093]

55. Trnka MJ, Baker PR, Robinson PJ, Burlingame AL, Chalkley RJ. Matching Cross-linked Peptide Spectra: Only as Good as the Worse Identification. Mol Cell Proteomics. 2014; 13(2):420–434. [PubMed: 24335475]

56. Soding J, Biegert A, Lupas AN. The HHpred interactive server for protein homology detection and structure prediction. Nucleic Acids Res. 2005; 33(Web Server issue):W244–248. [PubMed: 15980461]

57. Shen MY, Sali A. Statistical potential for assessment and prediction of protein structures. Protein Sci. 2006; 15(11):2507–2524. [PubMed: 17075131]

58. Chen ZA, et al. Architecture of the RNA polymerase II-TFIIF complex revealed by cross-linking and mass spectrometry. Embo J. 2010

59. Pontius J, Richelle J, Wodak SJ. Deviations from standard atomic volumes as a quality measure for protein crystal structures. J Mol Biol. 1996; 264(1):121–136. [PubMed: 8950272]

60. Rotkiewicz P, Skolnick J. Fast procedure for reconstruction of full-atom protein models from reduced representations. J Comput Chem. 2008; 29(9):1460–1465. [PubMed: 18196502]

Highlights

- PDE6 is regulated by the binding of inhibitory Pγ and noncatalytic cGMP.
- GAFab domains of the α- and β-subunit interact in a parallel orientation.
- Two catalytic domains swap and exist in an ‘open’ conformation.
- Pγ interacts with two noncatalytic cGMP binding sites in an asymmetric manner.

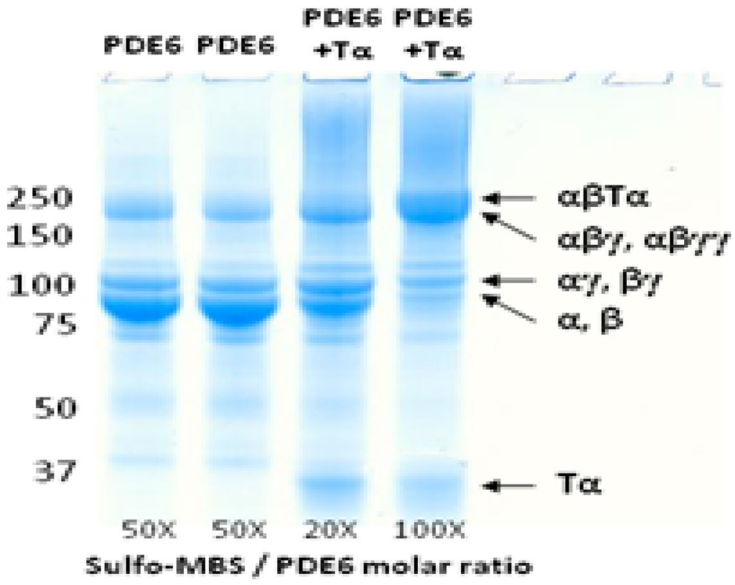

a

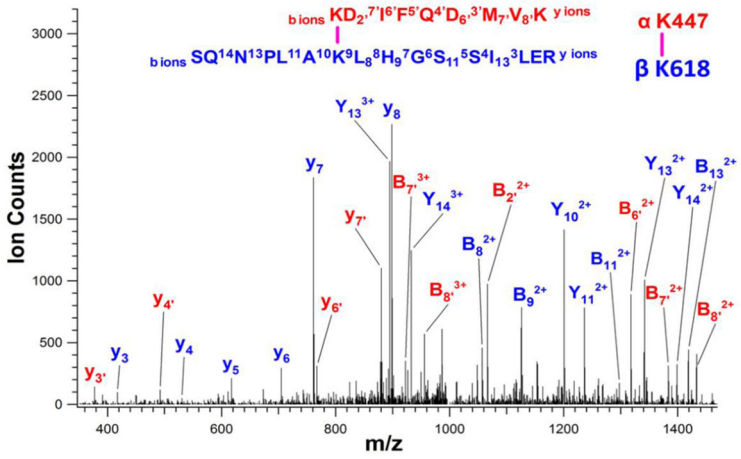

b

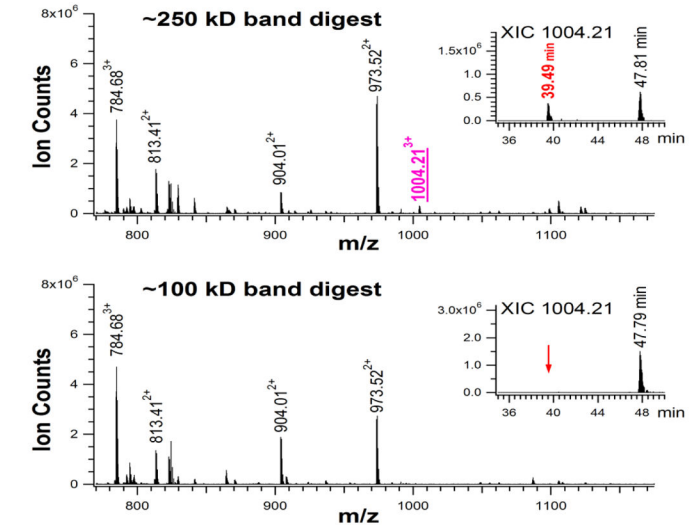

c

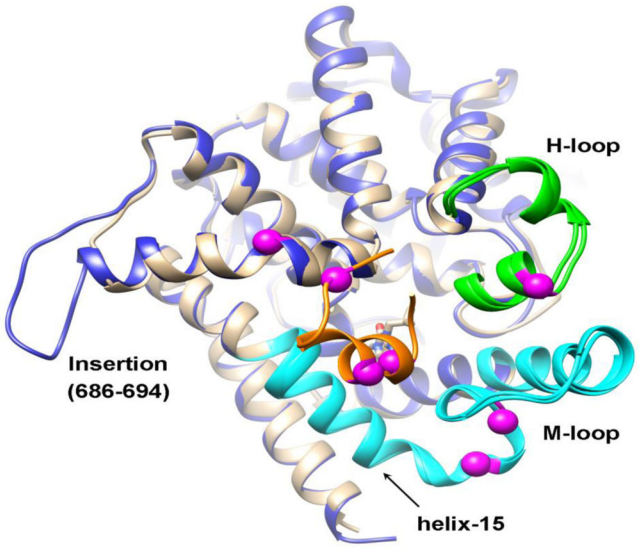

d

Figure 1.

Chemical cross-linking of the PDE6 holoenzyme. A) Purified PDE6 holoenzyme or the Pαβ catalytic dimer reconstituted with either wild-type (Pγ) or a quadruple lysine site-directed mutant of Pγ (Pγ4K) were cross-linked with BS3 or Sulfo-MBS. Control samples (Ctrl) were treated identically except that cross-linkers were omitted. Gel bands of uncross-linked subunits (γ and α/β) and cross-linked subunits (αγ or βγ at ~110 kD; αβ or αβγ or αβγγ at ~220 kD) are indicated. B) Tandem MS spectrum of a cross-linked peptide (at m/z 1004.21^{3+}) from the 220 kD band, with sequence fragments from both α-(K447-K455) and β-subunit (S612-K627). Sequence ion series from both peptide moieties identify the cross-link between Pα K447 and Pβ K618. Fragments with upper case labels contain the cross-

linked peptide moiety. C) Differential LC-MS analysis to determine the cross-linked peptide shown in Fig. 1B (at m/z 1004.21^{3+}) as an intersubunit cross-link. D) Superimposition of a comparative model for Pβ catalytic domain(*blue*) with the structure of chimeric PDE5/PDE6 catalytic domain (*gray*; PDB: 3JWR). H-loops are colored in green; M-loops and the α-helix 15 regions are colored in cyan. The C-terminal segment of Pγ in the PDE5/PDE6 chimera structure is colored in orange. Cross-linked residues between Pγ and Pβ that can be mapped in the structure are indicated as magenta spheres.

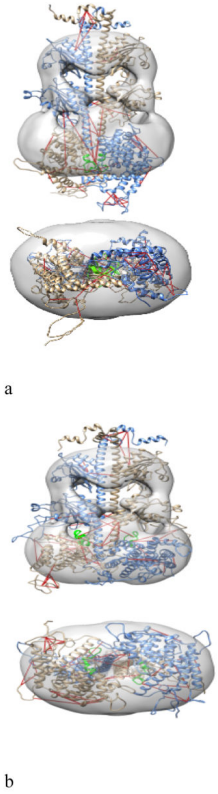

Figure 2.

Modeling of the PDE6 catalytic dimer. A) Homology model of the PDE6 catalytic dimer based on multiple template structures. B) A representative of the most populated cluster of Pαβ heterodimer models produced by the integrative modeling approach and structure refinement. The fit of PDE6 model in its EM molecular density map (12) is shown. *Bottom images* are of the catalytic domain viewed along the long axis of the catalytic dimer. H-loops are colored in green; cross-links are represented by red solid lines. The Pα and Pβ chains are represented by blue and light brown ribbons, respectively.

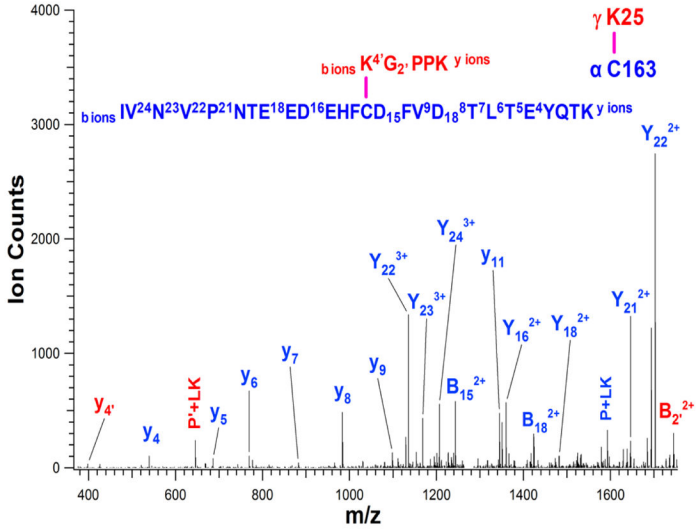

a

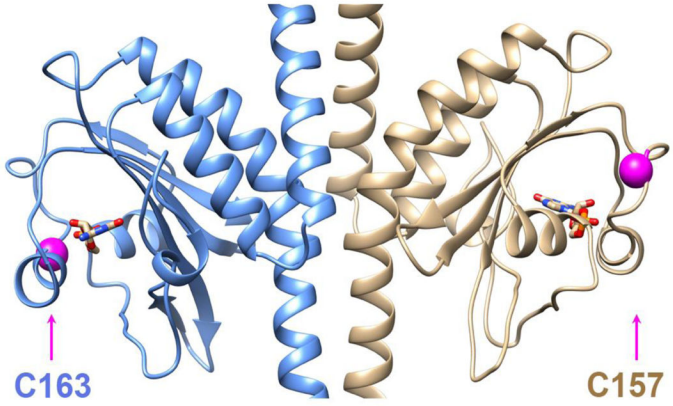

b

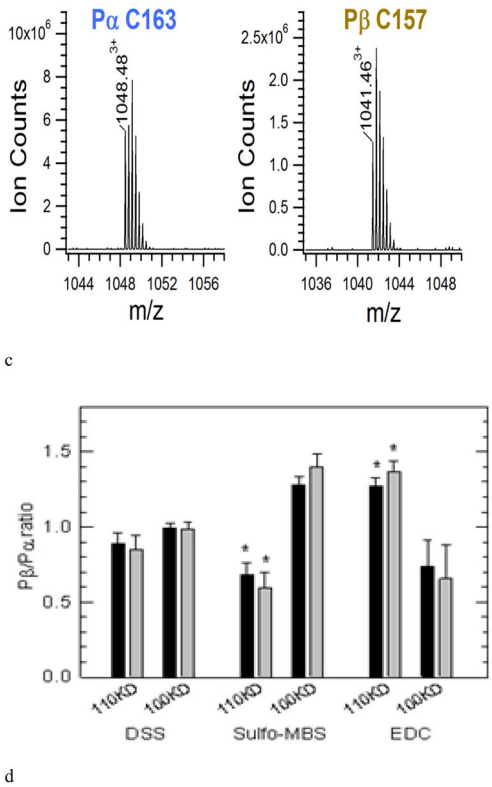

Figure 3.

Cross-linking preference of Pγ K25 for the α-subunit. A) Tandem MS spectrum of a Pγ peptide containing K25 cross-linked with Sulfo-MBS to a Pα peptide containing C163. B) Structural model of the GAFa domains of Pα (*blue*) and Pβ (*light brown*). C163 on the α–subunit is in close proximity to the 'lid' region of the noncatalytic cGMP (*ball and stick atoms*) binding site. Below is the sequence alignment of the bovine Pα and Pβ. C) MS analysis detected the unmodified tryptic peptides from both Pα (containing C163) and Pβ (containing C157). D) The reduction of Pβ in the Sulfo-MBS cross-linked 110 kD band, and the increase of Pβ in the EDC cross-linked 110 kD band. The number of unique peptide spectra (sequence discriminates Pα from Pβ; *gray*) as well as the number of total peptide spectra (*black*) for Pα and Pβ were determined to calculate the Pβ/Pα ratio. Statistical significance was evaluated by ANOVA analysis using Tukey's test (for 110 kD samples annotated with asterisks).

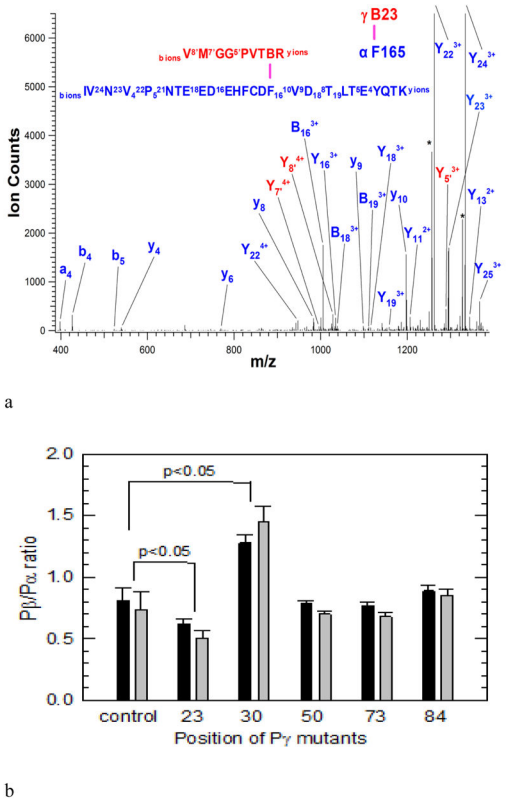

Figure 4.

Photoactivatable probes on Pγ reveal preferential interactions of Pγ with the α- or β-subunit of PDE6. A) Tandem MS spectrum reveals the cross-link between Pγ^{23}Bpa and Pα Phe^{165}. B) Pβ/Pα ratio for the number of peptide spectra identified in the 110 kD gel band with Pγ mutants: Pγ 23Bpa, Pγ 30C-MBP, Pγ 50C-MBP, Pγ 73C-MBP and Pγ 84C-MBP. The same region on the gel from a control sample not exposed to UV irradiation was processed for comparison. The number of unique peptide spectra (*gray*) and the number of total peptide spectra (*black*) for the α- and β-subunit were determined to calculate the Pβ/Pα ratio. Statistical significance was evaluated by ANOVA analysis using Tukey's test.

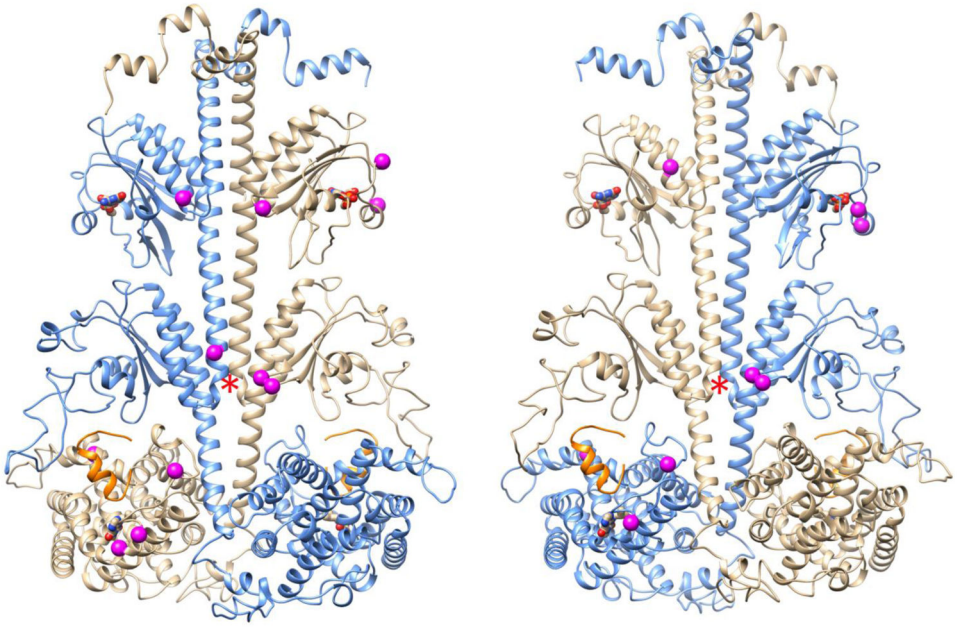

Figure 5.

Interaction surfaces of Pγ with the PDE6 catalytic dimer. The refined model for the PDE6 catalytic dimer (α-subunit, *blue*; β-subunit, *light brown*) was used to identify Pγ interacting sites on Pαβ. The front (*left*) and back (*right*) sides of Pαβ heterodimer are shown. Residues cross-linked with Pγ are represented as magenta spheres.

Table 1

Pαβ inter-subunit cross-linked peptides[a].

Exp. m/z	z	Cross-linked residues	Cross-linker	Δ (ppm)
1176.0327	4	Pα K21 - Pβ K26	DSS	−5.1
1149.5033	4	Pα K21 - Pβ C44	Sulfo-MBS	1.2
785.931	4	Pα K21 - Pβ K78	BS(PEG)5	−0.3
976.9792	4	Pα K31 - Pβ K26	DSS	9.9
727.4556	3	Pα K31 - Pβ K78	DSS	−0.3
1219.3896	4	Pα K76 - Pβ K184	BS(PEG)9	8.5
925.7562	4	Pα K247 - Pβ K391	DSS	0.0
1017.5593	4	Pα K393 - Pβ K245	BS(PEG)9	6.9
1042.8746	3	Pα K447 - Pβ K392	BS(PEG)9	−2.4
722.3749	3	Pα K447 - Pβ K440	DSS	−2.4
1004.2099	3	Pα K447 - Pβ K618	DSS	−3.6
824.2327	5	Pα K459 - Pβ K618	BS(PEG)9	−0.7
1034.5543	4	Pα K613 - Pβ K315	BS(PEG)9	0.7
658.6262	4	Pα K677 - Pβ K315	BS(PEG)9	−2.5

[a]Exp. *m/z* is experimentally measured mass-to-charge ratio. Z indicates the charge state of a cross-linked peptide. Its mass accuracy (Δ) was measured in parts-per-million (ppm).

Table 2

Intra-subunit Cross-linked peptide of PDE6[a]

Exp. *m/z*	*z*	Cross-linked residues	Cross-linker	Δ (ppm)
818.4393	4	Pα K21 - Pα K31	DSS	−5.1
872.4365	4	Pα K76 - Pα K84	DSS	1.4
1176.5813	1	Pα K76 - Pα K83	DSS	−3.0
1085.8302	4	Pα K247 - Pα K326	BS(PEG)9	−1.4
847.1967	4	Pα K284 - Pα K394	BS(PEG)9	−1.3
925.8341	3	Pα K393 - Pα K394 (Pβ K391 - Pβ K392)	DSS	−9.1
868.2375	4	Pα K393 - Pα K620 (Pβ K391 - Pβ K618)	BS(PEG)9	2.8
551.8272	4	Pα K534 - Pα K581	DSS	−2.0
704.3875	6	Pα K534 - Pα K579	BS(PEG)9	0.2
651.5932	4	Pα K613 - Pα K677 (Pβ K611 - Pβ K675)	BS(PEG)9	−3.3
800.4162	4	Pα K613 - Pα K765	BS(PEG)9	−0.6
588.9926	3	Pα K677 - Pα K683	DSS	−3.7
671.3542[b]	3	Pα K765 - Pα K827	DSS	−3.3
771.4012	4	Pα K786 - Pα K807 (Pβ K784 - Pβ K805)	DSS	2.7
846.6952	4	Pα K819 - Pα K821	DSS	−2.8
799.4021	3	Pα K819 - Pα K827	DSS	−3.3
846.6852	4	Pα K827 - Pα K829	DSS	−2.8
850.9222	4	Pα K827 - Pα K845	DSS	−5.0
642.5875	4	Pβ K392 - Pβ K440	DSS	−0.2
895.7186	4	Pβ K487 - Pβ K532	BS(PEG)9	−2.1
665.4031	4	Pβ K490 - Pβ K532	DSS	−1.9
762.2306	6	Pβ K490 - Pβ K579	BS(PEG)9	−1.8
953.5271	4	Pβ K490 - Pβ K577	BS(PEG)9	−0.6
671.1187	4	Pβ K532 - Pβ K577	BS3	−3.5
740.2131	6	Pβ K532 - Pβ K579	DSS	0.1
818.2048	4	Pβ K532 - Pβ K693	BS(PEG)5	9.4
589.3201	3	Pβ K675 - Pβ K681	DSS	−3.4
682.6841[b]	3	Pβ K687 - Pβ K784	BS3	−2.6
609.5557	4	Pβ K687 - Pβ K805	BS(PEG)9	−2.7
561.8072	4	Pβ K763 - Pβ K817	DSS	−2.3
860.4412	2	Pβ K805 - Pβ K808	DSS	−2.8
778.7425	3	Pβ K817 - Pβ K826	BS3	2.3
684.3658	3	Pβ K817 - Pβ K832	DSS	−3.8
681.5793	4	Pβ K817 - Pβ C839	Sulfo-MBS	0.1
773.0762	3	Pβ K819 - Pβ K826	DSS	3.2
501.2818	4	Pβ K819 - Pβ K832	DSS	0.7

Exp. *m/z*	*z*	Cross-linked residues	Cross-linker	Δ (ppm)
639.0802	4	Pβ K826 - Pβ K833	DSS	0.5
586.3139	3	Pβ K827 - Pβ K832	DSS	−2.3
1062.5453	2	Pβ K832 - Pβ C833	DSS	3.7
722.0148	3	Pβ K832 - Pβ C839	Sulfo-MBS	−1.9

[a] Tryptic peptides are listed unless otherwise indicated. Exp. *m/z* is experimentally measured mass-to-charge ratio. Z indicates the charge state of a cross-linked peptide. Its mass accuracy (Δ) was measured in parts-per-million (ppm).

[b] The cross-linked peptide is identified from a chymotryptic digestion.

Table 3

Pγ peptides cross-linked to the α- or β-subunit of PDE6[h].

Exp. m/z	z	Cross-linked residues	Cross-linker	Δ (ppm)
1188.2521	3	Pγ K7 - Pα K76	DSS	−1.1
784.4545	3	Pγ K7 - Pβ K78	DSS	−1.3
1115.5153	4	Pγ K7 - Pβ E156	EDC	1.0
735.3842	3	Pγ K7 - Pβ D169	EDC	−0.2
1053.2456	4	Pγ Bpa23[a] - Pα F165/V166	UV	9.6
957.9488	4	Pγ K25 - Pα C163	Sulfo-MBS	−0.8
463.9878	4	Pγ C38[b] – Pα K393 (Pβ K391)	Sulfo-MBS	−0.1
630.6078	4	Pγ K39 - Pα K393 (Pβ K391)	BS(PEG)5	−2.4
745.6680	4	Pγ K39 - Pα K326 (Pβ K324)	BS(PEG)9	−1.3
844.9681	4	Pγ K41 - Pβ K184	BS(PEG)9	−1.9
793.1881	4	Pγ K41 - Pα K247	DSS	−0.4
646.0474	3	Pγ K41 - Pα K393 (Pβ K391)	DSS	−5.8
727.1652	4	Pγ K44[c] - Pα K326 (Pβ K324)	DSS	−1.6
694.0745	3	Pγ K44[c] - Pα K393 (Pβ K391)	DSS	−5.2
739.6510	4	Pγ K45[d] - Pα K326 (Pβ K324)	BS(PEG)9	0.3
1072.0592	4	Pγ K45[e] - Pβ K184	BS(PEG)9	−2.7
871.6909	4	Pγ K45[c] - Pα K394 (Pβ K392)	DSS	−1.3
804.9171	4	Pγ K45[c] - Pα K393 (Pβ K391)	DSS	−5.5
932.2418	2	Pγ K53[d] - Pα K326 (Pβ K324)	BS(PEG)9	0.2
861.2065	4	Pγ K53[d] - Pα K393 (Pβ K391)	BS(PEG)9	−1.9
742.8607	4	Pγ C68[f] - Pα K613 (Pβ K611)	Sulfo-MBS	−4.1
488.9138	3	Pγ C68[f] - Pα K677 (Pβ K675)	Sulfo-MBS	−2.4
545.0488	4	Pγ K73[f] - Pα K677 (Pβ K675)	BS3	−7.6
900.9794	4	Pγ K79[f] - Pα K613 (Pβ K611)	BS3	6.3
694.3996	3	Pγ K79[f] - Pα K677 (Pβ K675)	BS3	4.3
703.8936	4	Pγ K79[f] - Pβ K763	BS(PEG)5	6.5
952.8429	3	Pγ K79[f] - Pβ K763	BS(PEG)9	−3.5
786.3686	4	Pγ C84[g] - Pα D762/R763	MBP/UV	3.7
786.6217	4	Pγ C84[g] - Pβ D760/R761	MBP/UV	8.9

[a] Cross-link from PDE6 reconstituted with Pαβ and Pγ23Bpa.

[b] Cross-link from PDE6 reconstituted with Pαβ and Pγ38C.

[c] Cross-link from PDE6 reconstituted with Pαβ and Pγ62K/65K.

[d] Cross-link from PDE6 reconstituted with Pαβ and Pγ53K/62K/65K/73K.

[e] Cross-link from PDE6 reconstituted with Pαβ and Pγ58K/62K/65K/73K.

[f] Cross-link from PDE6 reconstituted with Pαβ and Pγ62K/65K/73K/79K.

[g] Cross-link from PDE6 reconstituted with Pαβ and Pγ(1-84)62K/73K/84C-MBP.

[h] Exp. *m/z* is experimentally measured mass-to-charge ratio. Z indicates the charge state of a cross-linked peptide. Its mass accuracy (Δ) was measured in parts-per-million (ppm).